Close-Proximity Blast Loading and Damage of Cylinders

J.E. Slater, G. Rude, J.J. Lee

Defence Research and Development Canada (DRDC Suffield)
Suffield, AB, T1A8K6, Canada

Email: *julian.lee@drdc-rddc.gc.ca*

ABSTRACT

This paper describes an experimental study of underwater explosion (UNDEX) effects on responding targets at different depths and with varying charge standoff distances. Tests have been conducted on scaled generic targets consisting of aluminum cylinders with circumferential stiffeners machined on the inside or outside surface of the cylinders. Tests were also conducted on a thick-walled cylinder to provide an essentially non-responding target for comparison. To progressively increase the severity of the loading, the explosive charge was placed at three standoff distances: 1.0R, 0.6R and 0.2R where R is the maximum radius of the detonation product bubble; and the target was placed at three depths: shallow, intermediate, and on the bottom.

The purpose of the tests was to gain a better understanding of the complex near-field interaction of underwater blast and a responding cylinder target. By varying the standoff and depth, the proximity of the explosive charge to the various boundaries such as the target, the air surface and the bottom changed; thus producing a wide range of loading processes. The loading was found to consist of two main mechanisms: shock loading and water jet loading from the detonation bubble collapse. However, the loading history was strongly influenced by cavitation and cavitation closure reload.

1. INTRODUCTION

To develop effective countermeasures to protect naval ships and submarines against conventional military threats [1] and terrorist threats, it is necessary to assess the damage potential of close-proximity explosions. In particular, the critical charge weights and standoff distances (ie. Damage Radii) must be determined. Furthermore, the failure mechanism of the hull structure must be understood to assess structural integrity as well as vessel and crew survivability.

The UNDEX loading characteristics have been studied experimentally with flat, responding targets for small-scale [2] and medium-scale [3] plates. The loading response of these targets has also been analyzed and modeled in detail [4-5].

In the present study, underwater explosion tests were conducted for charges in close proximity to cylindrical targets to investigate the detailed loading and structural response. The targets consisted of small-scale cylinders of three types: rigid cylinder with thick, non-yielding walls; responding cylinder with thin walls and internal circumferential stiffeners; and responding cylinder with thin walls and external circumferential stiffeners. A number of scenarios were studied by varying the depth of the charge-target arrangement and the standoff distance of the charge. These tests revealed the complexity of the UNDEX loading and interaction with cylindrical targets.

2. EXPERIMENTAL DETAILS

The cylindrical targets were designed based on aluminum cylinder models previously used for determining static pressure collapse [6]. The targets were made from a single piece of 6061-T6 extruded aluminum tubing having material properties measured in previous tests [7] as shown in Table 1.

The three types of targets had the dimensions shown in Table 2. The length of all targets was 762 mm (30 in). The rigid cylinder had a relatively thick wall and was used for baseline tests where the motion of the target wall was minimal when subjected to UNDEX. The responding targets had thinner walls in comparison to study the influence of wall motion on the UNDEX loading. Two configurations of responding targets were made: internally-stiffened and externally-stiffened (Figure 1).

Elastic Modules	68.94 GPa	10 x 10^6 psi
Poisson's Ratio	0.33	0.33
Density	2700 kg/m^3	0.0975 lb/in^3
Yield Stress (at 0.2 Permanent Set Strain)	279 MPa	40,500 psi
Effective plastic strain at failure	0.12	0.12

Table 1. Mechanical Properties of the 6061-T6 Tube Material [7].

The stiffeners consisted of square circumferential ridges 5.5-mm wide, spaced 60.0 mm apart along the entire length of the cylinders. The diameter of the externally-stiffened target was slightly less than that of the internally-stiffened, thus increasing its structural rigidity.

Target	Outer Dia. (mm)	Inner Dia. (mm)	Wall Thickness (mm)	Stiffener Height (mm)
Rigid	252.7	228.6	12.1	n/a
Internally-stiffened	252.7	246.7	3.0	8.0
Externally-stiffened	234.6	228.6	3.0	8.0

Table 2. Summary of target dimensions.

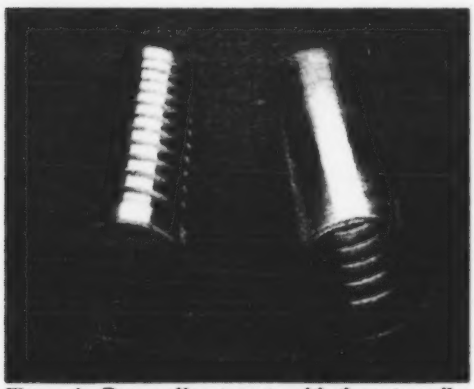

Figure 1. Responding targets with the externally-stiffened target on the left and internally-stiffened target on the right.

The targets were instrumented with gauges to measure the pressure on the target surface, the free-field pressure, the acceleration of the target mount, the dynamic displacement of the wall, and both the hoop and axial strain of the wall. After testing, the damage of the cylinder was assessed by measuring the radial and axial profiles of the UNDEX-generated dents in the wall.

The targets were mounted in a rig to place the explosive charge at various standoff distances from the wall (Figure 2). The standoff distances were chosen as a function of the maximum bubble radius as given by bubble radius similitude equation [8]:

$$R = k\left(\frac{W}{D+h}\right)^{1/3} \qquad (1)$$

where R is the maximum radius in meters, k is an empirical constant for a given explosive (a value of 3.76 m$^{4/3}$kg$^{-1/3}$ was used for RP-85 detonators in current tests),W is the explosive mass in kilograms, D is the charge depth in meters, and h is the local atmospheric pressure in meters of fresh water. Standoff distances of 0.2 R, 0.6 R, and 1.0 R were used in the tests. The explosive charge used throughout the tests was a Reynolds RP-85 detonator which contains 1.1 g of RDX explosive (including 0.08 g of PETN). Each test was filmed underwater using a high-speed video camera running at 1000 frames-per-second. The camera was protected against the underwater blast conditions by a shock-hardened enclosure.

Figure 2. Top view of submerged instrumented target cylinder in rig with detonator and underwater camera.

The tests were conducted in the UNDEX pond facility at DRDC Suffield which has a diameter of 50 m and a maximum depth of 8 m. Three depths of 0.15 m (shallow), 1.0 m (medium), and about 6.8 m (bottom) were used. For tests on the bottom, the target-charge arrangement was placed on top of concrete blocks located on the bottom of the pond.

3. RESULTS AND DISCUSSION

Over 70 tests were conducted with the three target types at different standoff distances and depths.

3.1 Shock and Bubble Loading

The UNDEX loading phenomena observed were of two types: shock loading, and bubble jet loading. The shock loading consisted of sharp pressure spike having the traditional triangular shape of an underwater blast wave (Figure 3). The pressure traces in Figure 3 are from three separate tests at different standoff distances. As expected, the peak pressure decreased as the standoff distance was increased. The shock pressure spikes were of short duration, typically lasting one to two hundred microseconds.

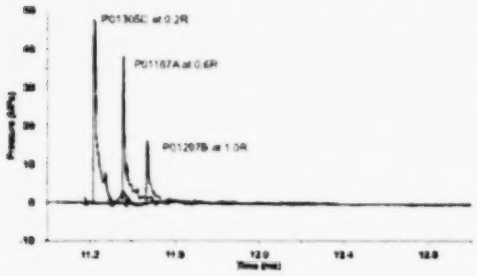

Figure 3. Free-field pressure traces for tests on an internally-stiffened cylinder at medium depth.

The second type of loading was due to the collapse of the bubble of gaseous detonation products. This well-known UNDEX phenomenon [9] causes a highly focused and directional jet of water to impinge upon nearby surfaces. This jet will be referred to as the bubble jet in this paper. Following collapse, the bubble re-expands and collapses again in a periodic manner. The pressure loading from the bubble jet appears as a pressure pulse a few tens of milliseconds after the initial shock. As shown in Figure 4, the pressure pulse from the first bubble collapse of an RP-85 detonator occurs about 30 ms after the shock. A second pressure pulse from a second bubble collapse is also observed.

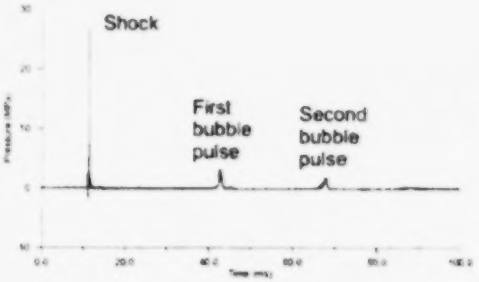

Figure 4. Free-field pressure history for a test at medium depth on an internally-stiffened target with the charge at a 1.0 R standoff distance.

For the current tests, the observed maximum bubble radius agreed well with similitude equations. The experimental maximum bubble radius is shown with the similitude equation (Eq. 1) correlation in Figure 5. The measured bubble radius from tests with all three types of targets (rigid, internally-stiffened, and externally-stiffened) are shown.

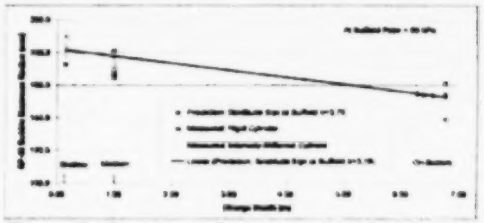

Figure 5. Experimental maximum bubble radii with similitude equation correlation.

The period for the first bubble was measured using interval between the time-of-arrival of the shock and the first bubble pulse (Figure 4). The experimental period was again compared with a similitude equation correlation [8]:

$$T = K \frac{W^{1/3}}{(D+h)^{5/6}} \qquad (2)$$

where T is the bubble period in seconds, K is a constant for a given explosive type (a value of $2.29\ kg^{-1/3}m^{5/6}s$ is used for RP-85 detonators in the current tests), W is the explosive charge mass in kilograms, D is the charge depth in meters, and h is the local atmospheric pressure in meters of fresh water. For charges in shallow water or near the bottom of the pond, it is necessary to add correction factors to Equation 2 [8-10].

$$T = K\frac{W^{1/3}}{(D+h)^{5/6}}\left[1-\frac{\alpha R}{D}\right]\left[1+\frac{\alpha R}{H}\right] \qquad (3)$$

where the additional variables are H, the charge height above the bottom in meters, and the constant α which has a value of 0.1 for R/D and R/H less than 0.5, and a value approaching 0.2 in shallow water. The similitude correlation of Equation 2 (dashed line in Figure 6) was found to diverge from the experimental bubble period at shallow water and on the bottom. However, the corrected similitude correlation of Equation 3 (solid line in Figure 6) showed an improved agreement with experiments.

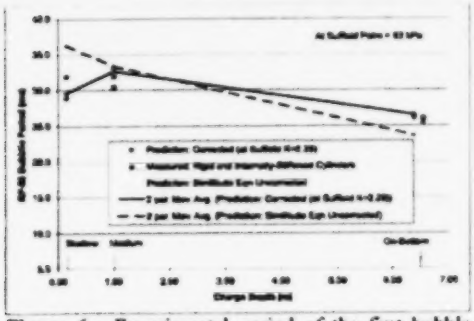

Figure 6. Experimental period of the first bubble compared to similitude equation correlation.

Cavitation was observed to strongly influence the pressure loading [9]. Cavitation was caused by rarefaction waves from the water-air interface at the surface or from the surface of a responding target. In the first case, shock reflection from the water-air interface produced a region of cavitated water just below the surface. In the second case, pressure loading of the target surface caused the wall to recede and produce a region of cavitated water near the target surface. The occurrence of cavitated water essentially eliminated the pressure field, as shown in Figure 7. This cavitation cutoff thus altered the pressure history, and consequently changed the pressure loading on the responding targets. Another possible effect of cavitation was cavitation closure reload, where the pressure field in the water was suddenly restored when the cavitation bubbles collapsed.

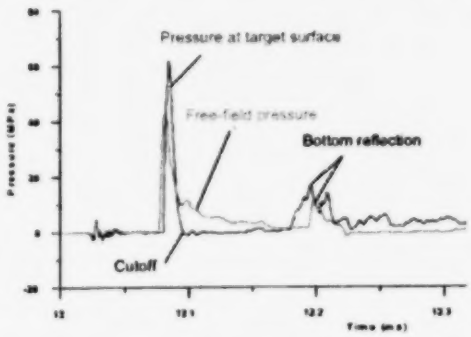

Figure 7. Free-field pressure and target surface pressure for an internally-stiffened target at the bottom with a charge standoff distance of 0.2R.

The shock and bubble jet loading dynamics is illustrated in a sequence of high-speed movie frames (Figure 8). This sequence shows the ignition of the detonator and growth of the detonation product bubble at 1 and 2 ms. The shock loading of the target occurs within the first couple hundred microseconds, but is not visible in the video. At 4 ms, a diffuse cloud forms near the target, indicating the appearance of a cavitation field due to motion of the target wall. From 6-19 ms, the bubble continues to grow, coming into contact with the target. From 22-32 ms, the bubble collapses towards the target, causing bubble jet loading.

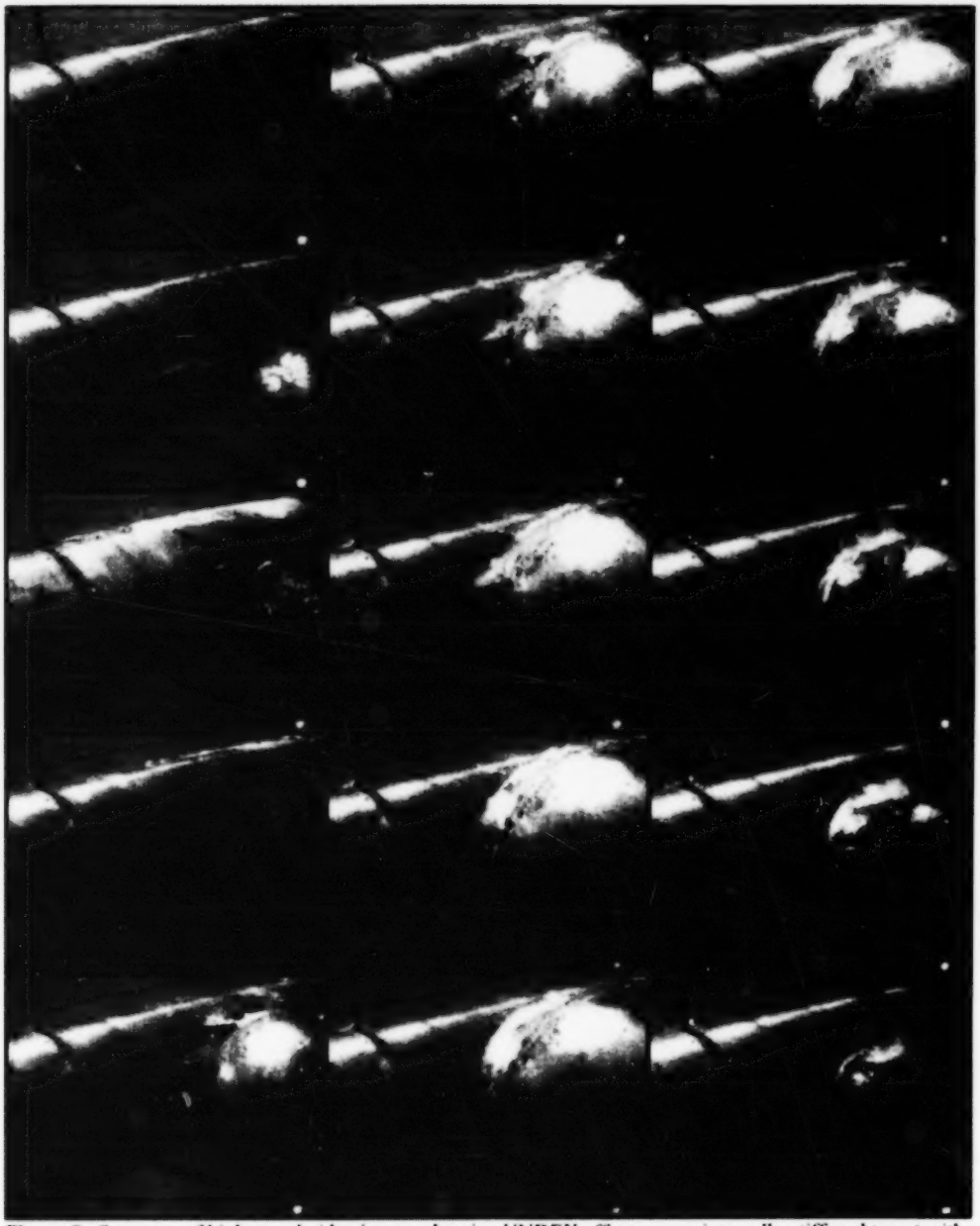

Figure 8. Sequence of high-speed video images showing UNDEX effects on an internally-stiffened target with the charge at a 0.6 R standoff distance. The test was conducted at a medium depth. The time between the frames is not uniform.

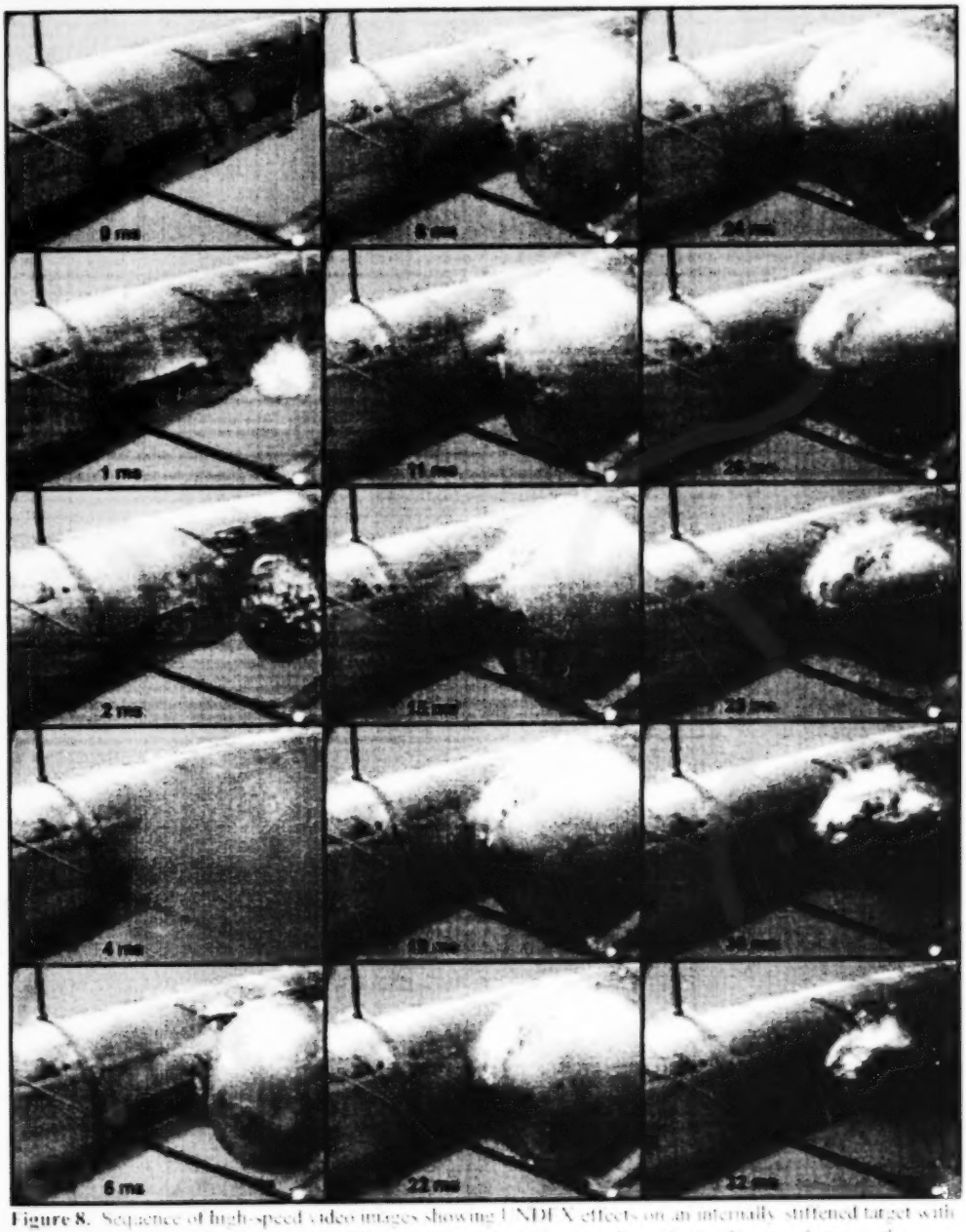

Figure 8. Sequence of high-speed video images showing UNDEX effects on an internally stiffened target with the charge at a 0.6 R standoff distance. The test was conducted at a medium depth. The time between the frames is not uniform.

3.2 Depth Effects

Results showed that at shallow depth, the UNDEX loading was strongly influenced by the water-air interface. Due to the close proximity of the charge to the surface, the bubble would break through and allow product gases to freely flow out of the bubble and air to flow back in. This strongly reduced the strength of the bubble jet to the extent that no significant pressure rise was observed where a bubble jet pulse was expected. A periodic bubble collapse phenomenon was still observed in high-speed video images, but at a much weaker intensity. Shock reflection from the interface also produced a large cavitation field near the surface. Although the cavitation was clearly visible in high-speed movies, it was unclear if cavitation cutoff had significantly affected the pressure loading. The free surface also caused the bubble to migrate away from the surface, resulting in bubble jet loading moving towards the lower part of the target.

At medium depth, the targets were subjected to both shock and bubble jet loading near the point of attack. Since the target-charge arrangement was at a relatively large distance from both the free boundary at the surface and the rigid boundary at the bottom, the bubble was drawn straight towards the target. There was however a small upwards migration of the bubble due to buoyancy.

For tests on the bottom, the UNDEX loading was strongly influenced by the rigid bottom surface. The reflected shock from the bottom caused additional loading of the target (Figure 7). In addition, the rigid bottom caused a migration of the bubble towards the bottom, resulting in migration of the bubble jet loading towards the lower part of the target in contact with the bottom.

3.3 Standoff Effects

Tests at the three standoff distances (0.2 R, 0.6 R, and 1.0 R) showed three distinct structural responses. The response of the rigid cylinder was not measured, however since no permanent deformation was noted after testing, the response was assumed to be elastic. The structural response of both responding targets (internally-stiffened and externally-stiffened) was qualitatively the same.

At the largest standoff distance of 1.0 R, the responding targets suffered no significant permanent damage. Displacement measurements at the target wall typically showed two or three distinct spikes (Figure 9). The first spike was due to shock loading, the second was due to the bubble jet from the first collapse, and the third was due to the bubble jet from the second collapse. The third spike did not appear in all tests. Following this pressure loading and response of the target, the displacement returned to zero indicating an essentially elastic response.

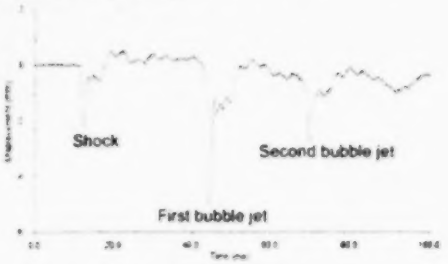

Figure 9. Displacement history for an internally-stiffened target at medium depth with a charge at a standoff distance of 1.0 R.

At the intermediate standoff distance of 0.6 R, the displacement measurements again showed three distinct spikes (Figure 10). However, only the loading from the first bubble jet was strong enough to cause permanent deformation since the shock only produced an elastic response. Post test inspection of the target indeed showed a dent in the target at the attack point of the charge. At this standoff, the pressure loading was thus dominated by the first bubble jet.

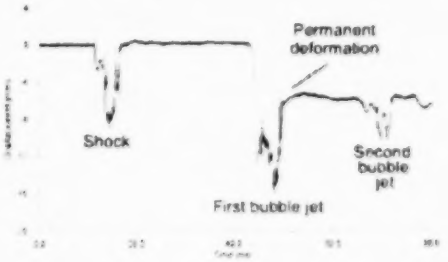

Figure 10. Displacement history for an internally-stiffened target at medium depth with a charge at a standoff of 0.6 R.

At the closest standoff of 0.2 R, permanent deformation was observed for both the shock pulse and the first bubble pulse. The displacement caused by the shock was found to be 2-3 times larger than that produced by the bubble jet (Figure 11). Hence at this standoff distance, the loading appeared to be dominated by the shock.

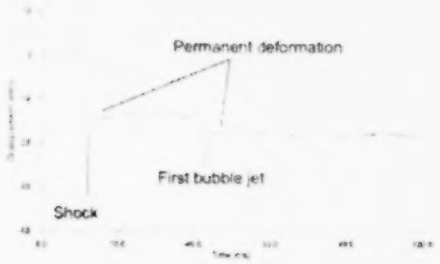

Figure 11. Displacement history for an internally-stiffened target at medium depth with a charge at a standoff of 0.2 R.

At shallow depth, this loading phenomenon was different, as the bubble jet was weakened from breaching the surface. The loading was consequently dominated by the shock at all standoff distances.

For the largest depth at the bottom, the bubble was attracted to the rigid bottom surface, thus diverting the bubble jet away from the target. The loading was thus dominated by the shock.

3.4 Damage

Damage to the responding targets was observed in the form of a dent in the wall at the attack point of the explosive charge (Figure 12), i.e. the point on the target wall closest to the charge. To evaluate the severity of the damage, the depth profile of the dents was measured. As the standoff distance of the charge decreased, the maximum depth of the dents increased, indicating that damage was strongly dependent on shock loading.

In addition, the dents in internally-stiffened targets were found to be approximately 15% deeper than in externally-stiffened targets. Because the externally-stiffened targets had a slightly smaller diameter than the internally-stiffened targets (Table 2), they were expected to be more rigid. Conclusions could not be drawn as to whether the difference in dent depth was due to the difference in diameter, or to the stiffeners being external or internal.

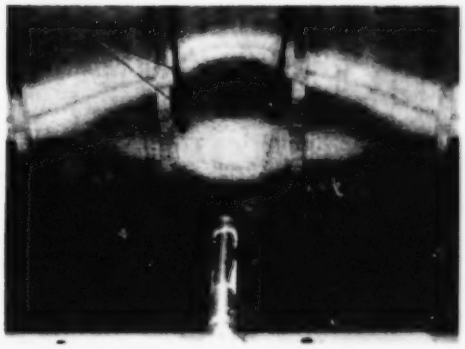

Figure 12. Dent in an externally-stiffened target.

4. Summary and Conclusions

The current UNDEX tests showed the two main loading mechanisms to be the shock and the bubble jet. Through a systematic investigation of various depths and charge standoff distances, we have observed the influence of boundaries on the loading phenomena.

At shallow depth, the bubble broke out of the surface and the bubble jet was severely weakened. The loading was thus dominated by the shock. The surface also acted as a free boundary that repelled the bubble and caused a downward migration.

At medium depth, the UNDEX loading was essentially free from the influence of the free boundary at the surface and the rigid boundary at the bottom, and both shock and bubble jet loading contributed to the deformation of the target.

At maximum depth on the bottom, the bubble jet was diverted away from the target by attraction to the rigid bottom surface, resulting in shock-dominated loading.

Varying the standoff distance of the charge showed the influence of target response on the pressure loading. Under shock loading, the recession of the responding target wall generated expansion waves that in turn generated a cavitation field. The main effect of cavitation was the elimination of pressure loading. A secondary effect was cavitation closure reload where the pressure loading was suddenly restored and increased by the collapse of the cavitation field. As expected, the shock loading decreased in magnitude as standoff distance increased. It was also found that varying the standoff distance yielded two loading regimes: a

shock dominated regime at small distances, and a bubble jet dominated regime at medium distances.

The investigation of damage to the responding cylinders showed that permanent deformation was strongly dependent on shock loading.

The present investigation has illustrated the complexity of the UNDEX loading on responding structures, and the strong influence of boundaries on the shock and bubble phenomena. The case of shallow charges is particularly complex, as it involves interactions with the spray dome, the cavitation field, and venting of the bubble into the air. This leads to a complex partitioning of the explosion energy between the water and the air. Further investigation of the near-surface effects is necessary to understand the mechanisms of bubble venting, surface breakup into droplets, and interactions with surface cavitation fields. In addition, many issues with the structural response and particularly damage mechanisms of responding targets remain as yet unresolved.

ACKNOWLEDGEMENTS

The authors gratefully acknowledge the assistance of the field operations personnel, and well as the instrumentation support of D. Boechler and M. Hickey.

REFERENCES

[1] Chick, M., Taylor, L.C., Evans, E. and Slater, J.E. Key Task1-28: Underwater Explosive Effects for Sea Mine Neutralization. (TTCP Technical Report LRTR-WPN-1-1999). The Technical Cooperative Program, 1999.

[2] Slater, J.E. and Rude, G., Experimental Study of Fluid-Structure Interaction during Close-Proximity Underwater Explosions. In *Proceedings of the ASME PVP Conference*, Vol 325, 1-10. Montreal, QC. ASME, 1996.

[3] Slater, J.E. and Rude, G., Loading and Response of Flat Plate Targets from Close-Proximity Underwater Explosions. In *Proceedings of the 71st Shock & Vibration Symposium*. Arlington, VA. SAVIAC, 2000.

[4] Link, R., Jiang, L., and Slater, J.E. Numerical simulation of the Loading and Response of Flat Plate Targets Subjected to Close Proximity Underwater Explosions. In *Proceedings of the 75th Shock & Vibration Symposium*. Virginia Beach, VA. SAVIAC, 2005.

[5] Buckland, M. and Slater, J.E. Analysis of the Structural Response of a Flat Plate Target to the Shock and Bubble Loading from Close-Proximity Underwater Explosions. In *Proceedings of the 8th International Symposium on Interaction of the Effects of Munitions with Structures*. Washington DC. DSWA, 1997.

[6] Pegg, N.G., Bosman, T.N. and Keuning, P.J. Summary Report on the Canada/Netherlands Project on Determination of Overall Collapse of Imperfect Pressure Hull Compartments. (DREA Report 94/101). Defence Research Establishment Atlantic, 1994.

[7] McKirgan, J. Characterization of Aluminum 6061-T6 Tube for High Rate Loading Applications. (NSWCCD-61-TR-2003/17). Naval Surface Warfare Center, Carderock Division, Bethesda, MD, 2004.

[8] Swisdak, M.M. Explosion Effects and Properties: Part II - Explosion Effects in Water. (NSWC/WOL/TR-76-116). Naval Surface Weapons Center, White Oak, MD, 1978.

[9] Cole, R.H. Underwater Explosions. Princeton University Press, 1948.

[10] Snay, H.G. Underwater Explosion Phenomena: The Parameters of Migrating Bubbles. (U.S. NAVORD Report 4185). Naval Ordnance Laboratory, White Oak, MD, 1962.